Chaos, Solitons and Fractals 171 (2023) 113439

Contents lists available at ScienceDirect

Chaos, Solitons and Fractals

journal homepage: www.elsevier.com/locate/chaos

Tipping time in a stochastic Leslie predator–prey model

Anji Yang [a], Hao Wang [b], Sanling Yuan [a,*]

[a] College of Science, University of Shanghai for Science and Technology, Shanghai 200093, China
[b] Department of Mathematical and Statistical Sciences, University of Alberta, Edmonton, AB T6G 2G1, Canada

ARTICLE INFO

Keywords:
Critical transition
Noise-induced tipping
Maximal likely trajectory
Tipping time
Fokker–Planck equation
Safe operating set

ABSTRACT

Critical transitions are usually accompanied by a decline in ecosystem services and potentially have negative impacts on human economies. Although some early warning signals based on a generic characteristic of local bifurcations, such as variance and autocorrelation, can be used to predict an imminent critical transition, studies have shown that these indicators are ineffective for purely stochastic transitions. In this paper, we propose to use the maximum likelihood state, based on the Fokker–Planck equation, to track the true state of a predator–prey model under noisy fluctuations. Then, we use the maximal likely trajectory to determine tipping times for the most probable transitions from a high biomass state to a low biomass one. Numerical results show that the tipping times of population collapse depend strongly on the noise intensity and the growth rate of predator. We uncover that the enhanced disturbance events promote ecosystem collapse and that an increase in predator growth rate significantly alleviates the influence, which is beneficial to the stability and biodiversity of an ecosystem. Based on this, we define a two-dimensional region, called the Safe Operating Set (SOS) of the population ecosystem. SOS boundary exhibits a trade-off such that increased predator growth rates can compensate to some degree for losses from environmental perturbations. To verify the above conclusions, we fix noise intensity and calculate the quasi-potentials of the corresponding high biomass state for different predator growth rates. We can see that the results for measuring the stability of the high biomass state derived from the perspective of quasi-potential are consistent with the results obtained from the analysis of tipping time.

1. Introduction

In complex ecosystems, critical transition (regime shift) refers to the state of a system suddenly flipping from its current state to a contrasting state when external inputs pass a tipping point [1]. These transitions are usually irreversible tipping events, and may cause unexpected catastrophic consequences. Examples of such sudden transitions are common in nature [2–5], including the collapse of global fisheries [6] and large African mammals (such as the Syncerus caffer) [7], and a dramatic reduction in penguin and sardine populations [8]. In addition, some abrupt transitions will directly threaten human survival and development, such as tempestuous declines in crop yields due to extreme weather [9]. Therefore, it is meaningful to identify and clarify the potential mechanisms of these critical transitions. Current studies on tipping effects primarily focus on the following three common tipping mechanisms [10]:

- Bifurcation-induced tipping (B-tipping): the situation when the time-varying parameter of a system approaches a bifurcation point, where the system is vulnerable, and even weak disturbances can cause dramatic changes in the state [11–13].
- Rate-induced tipping (R-tipping): the situation where a system moves too far away from its moving equilibrium point on account of rapid changes in time-varying parameters [10,14,15].
- Noise-induced tipping (N-tipping): the situation when the intensity of the external random disturbance exceeds a certain critical value, the random trajectory escapes from the basin of the attraction of a base state and enters the domain of attraction of a distinct state [16–18].

Notice that all of the tipping mechanisms mentioned above are model-based, i.e., the model structure has a significant impact on the results. Recently, some seminal works of detecting tipping point based on data have been reported. For example, Ref. [19] developed a model-free approach to detect change points in time series data recorded by real systems. Ref. [20] predicts tipping points in the system based on data using a machine learning approach.

In reality, numerous complex ecosystems are embedded in highly noisy environmental conditions. For instance, by analyzing high–frequency monitoring data of Lake Mendota, Carpenter et al. [21]

* Corresponding author.
E-mail address: sanling@usst.edu.cn (S. Yuan).

https://doi.org/10.1016/j.chaos.2023.113439
Received 19 December 2022; Received in revised form 23 March 2023; Accepted 3 April 2023
Available online 12 April 2023

found that stochasticity can push the random switching of phycocyanin between high and low concentrations. Blasius et al. [22] conducted an experimental predator–prey ecosystem, and the results revealed that stochasticity may lead to a reversible transition from coherent to non-coherent oscillations. In this paper, we will probe the effect of environmental stochasticity on a predator–prey model of noise-induced tipping.

For the bifurcation-induced tipping mechanism, as the environmental conditions approach a tipping point, the resilience of the system will change. In this case, the slightly perturbed system returns to its previous state at a slower rate [12]. We refer to this hallmark as "critical slowing down (CSD)" in dynamical systems theory [12], and an array of statistical metrics based on CSD are mentioned to as generic early warning signals (EWS) [23], which can give managers some hints before an approaching tipping point and avert an undesirable state shift. However, Hastings et al. [24] have illustrated that EWS are disabled for purely stochastic transition from one stable basin to another in highly random environments. In this circumstance, it may be better to implement nonparametric models [25] or threshold autoregressive models [26] to monitor upcoming transitions. In addition, as is well known, the solution of a stochastic model is a stochastic process, and the stochastic system can generate a large number of sample trajectories for a given initial value in the phase plane, which could hardly offer useful information for understanding the system's dynamics [27]. Therefore, the identification of the most probable position of the solution trajectory starting from near the equilibrium point in every moment is a key step to explore such an abrupt transition [28]. To this end, we focus on the maximal likely tipping path, based on the Fokker–Planck equation, for a predator–prey model under the noise perturbations.

In multistable systems, external stochastic forces can flip a system from one attractor to another. Several available methods are proposed to capture such transition paths in stochastic systems and implemented in various fields. For instance, Zheng et al. [28], based on the solution of the nonlocal Fokker–Planck equation, investigated the maximum likelihood climate change of an energy balance system under the extreme climate events, and found that the cold climate state suddenly shifts to the warm climate state owing to the presence of noisy fluctuation. Yang et al. [29] studied the sudden change of maximum likelihood state in a random thermohaline circulation system. Another work of theirs is to consider the disaster-happening tipping time of the maximal likely trajectories for an Arctic sea ice system subject to the disturbance of extreme weather events [30]. Moreover, Cheng et al. [31] applied the tool of maximal likely trajectories to a genetic regulatory system, and their results provide insights for further medical research.

It is worth emphasizing that the above mentioned works associated with the maximum possible trajectories are considered in a one-dimensional model. At present, no one has studied the mechanism of ecosystem collapse utilizing the maximum possible trajectories. Similar to [32], in this study, we call the time when the most likely trajectory collapse suddenly from the high biomass to the low biomass as the tipping time. We will scrutinize the impact of the intensity of disturbance events on the disaster-happening tipping time of ecosystems. Currently, most of the concepts of stability have been developed in a deterministic framework, such as linear stability analysis. These can be misleading when applied to stochastic dynamical systems with alternative states since stochastic perturbations may lead to shifts between states [33]. Therefore, we also expect that the most probable tipping time serves as a valid indicator to measure the stability of high biomass equilibrium points. We believe that the larger the value of tipping time, the stronger the stability of the high biomass equilibrium point. In addition, we also compute another metric for the stability of attractors in stochastic dynamical systems, the quasi-potential, to validate the metric we propose here.

The paper is structured as follows. In Section 2, we introduce a predator–prey model driven by Gaussian white noise. In Section 3 we validate the numerical method of obtaining the probability density function by Monte Carlo simulations. A detailed numerical method for solving the probability density function is presented in Appendix B. In Section 4, we examine the effects of Gaussian white noise on the transition behavior of the high biomass. The disaster-happening tipping time of the predator–prey model is also calculated in this section. The meanings of our results are discussed in Section 5.

2. Model

In this paper, we consider the following stochastically forced predator–prey model of Leslie type with generalized Holling type III functional response:

$$\begin{aligned} \mathrm{d}x &= \left[rx\left(1-\frac{x}{K}\right)-\frac{mx^2y}{ax^2+bx+1}\right]\mathrm{d}t+\sigma_1 x\mathrm{d}B_1,\\ \mathrm{d}y &= sy\left(1-\frac{y}{hx}\right)\mathrm{d}t+\sigma_2 y\mathrm{d}B_2, \end{aligned} \tag{2.1}$$

where $x(t)$ and $y(t)$ are respectively the population densities of the prey and predator at time t. In the absence of predators, the prey exhibits logistic growth with an intrinsic growth rate r and a carrying capacity K. In the presence of predators, the predators prey on their prey according to the generalized Holling type III functional response function $\frac{mx^2}{ax^2+bx+1}$ (See Appendix A for detailed introductions on Holling type response functions). Moreover, the predator population grows logistically with an intrinsic growth rate s, and its carrying capacity is assumed to be proportional to the biomass of the prey population, that is hx where the parameter h measures the food quality of the prey for conversion into the predator growth. The parameters r, K, m, a, s and h are positive constants, and $b > -2\sqrt{a}$ (so that $ax^2+bx+1>0$ for all $x > 0$). $B_1(t)$ and $B_2(t)$ are Wiener processes whose formal derivatives are Gaussian white noise processes, positive constants σ_1 and σ_2 denote the noise intensities. For the simplicity of discussion, we assume $\sigma_1=\sigma_2=\sigma$.

When $\sigma = 0$, i.e., without stochastic interferences, model (2.1) is reduced to the following deterministic model:

$$\begin{aligned} \frac{\mathrm{d}x}{\mathrm{d}t} &= rx\left(1-\frac{x}{K}\right)-\frac{mx^2y}{ax^2+bx+1},\\ \frac{\mathrm{d}y}{\mathrm{d}t} &= sy\left(1-\frac{y}{hx}\right), \end{aligned} \tag{2.2}$$

which has ever been considered in Refs. [34,35]. It is shown there that the model can exhibit complex dynamics such as various bifurcations and multi-type bistability phenomena. Take the following set of parameter values [34]:

$$r=1, h=1, b=-1.65, K=10, a=1.25, m=0.54, s=0.5. \tag{2.3}$$

Then model (2.2) has two stable equilibria: $E_1 = (1,1)$ and $E_3 = (4,4)$, which correspond respectively to a low biomass state and a high biomass state; and one saddle point $E_2 = (2,2)$. Fig. 2.1 shows the phase portraits of model (2.2) for this set of parameter values. The separatrices of the basins of attraction of two stable attractors are indicated by dashed red lines. Obviously, the solution trajectories of model (2.2) starting near the equilibrium points E_1 and E_3 converge respectively to the attractors E_1 and E_3.

Although deterministic models can successfully capture certain characteristics of population dynamics, a realistic feature of predator–prey dynamics is its variability due to external fluctuations [36]. Now we consider the case when $\sigma \neq 0$ and scrutinize the influence of environmental noise on population dynamics. We take the same parameter values as in Fig. 2.1 and set the noise intensity $\sigma = 0.045$. Fig. 2.2 displays the stochastic trajectory originated from the vicinity of E_3 will escape from its attraction basin enter the basin of attraction of equilibrium point E_1. This indicates that environmental fluctuations can trigger a regime shift (from the high biomass state to the low biomass state) in the population ecosystem and cause a sudden and unpredictable decrease in population size.

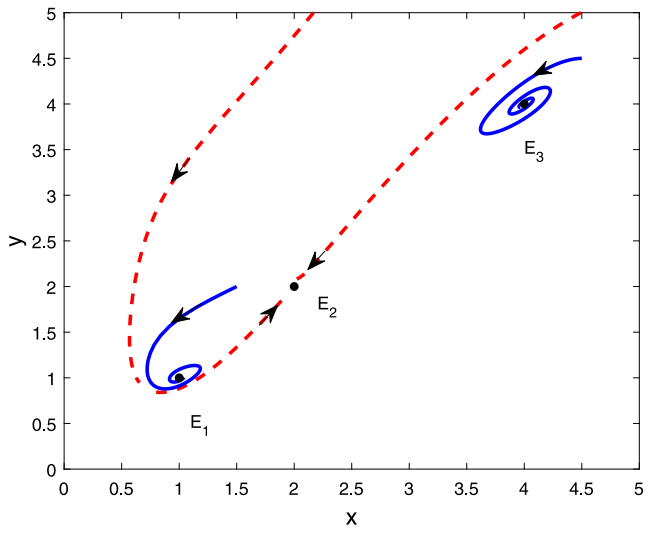

Fig. 2.1. Phase portraits of model (2.2) with parameters $r = 1$, $h = 1$, $b = -1.65$, $K = 10$, $a = 1.25$, $m = 0.54$ and $s = 0.5$. E_1, E_3 are stable equilibria and E_2 is unstable. The separatrices of the basins of attraction of two stable attractors are indicated by dashed red lines. (For interpretation of the references to color in this figure legend, the reader is referred to the web version of this article.)

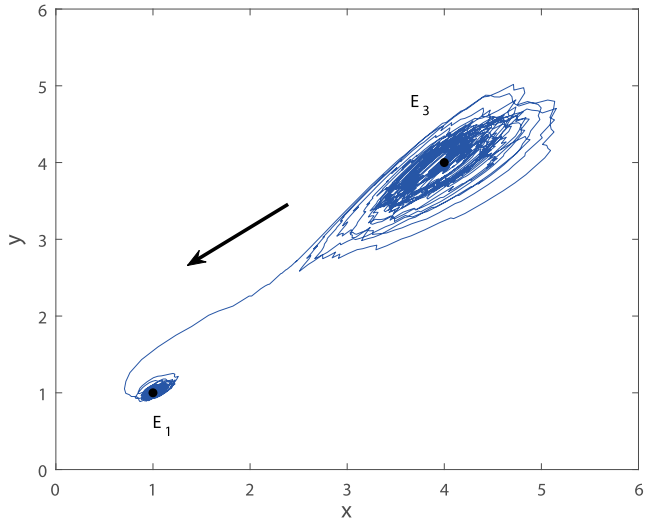

Fig. 2.2. The phase trajectories of stochastic model (2.1) with initial value $(4.1, 4.1)$ and noise intensity $\sigma = 0.045$.

In the sequel sections, we will investigate the effect of Gaussian white noise on the dynamics of predator–prey model (2.1) from the perspective of stationary probability density function (SPDF), which is one of the key tools for studying the stochastic dynamical behavior of models with multiple stable attractors. Specifically, we use the coordinates at the maximum of SPDF to track the true state of stochastic predator–prey model (2.1). Depending on the noise intensity, the SPDF of species biomass may have one or two peaks near the stable attractors, and the shape and height of the peaks determine the occupation probability of the corresponding attractor. Statistically, the greater occupation probability determines the final population size.

3. Numerical method

To obtain the most probable position of the solution trajectory at each moment, we need to solve the corresponding Fokker–Planck equation and then record the maximizer of probability density function at every time t. For the readability of the article, the detailed numerical method for solving the probability density function is provided in Appendix B.

To validate the numerical algorithm, we simulate the following formulas:

$$\begin{aligned} x_{\hat{n}+1} &= x_{\hat{n}} + f_1(x_{\hat{n}}, y_{\hat{n}})\Delta t + \sigma_1 x_{\hat{n}} \Delta B^1_{\hat{n}}, \\ y_{\hat{n}+1} &= y_{\hat{n}} + f_2(x_{\hat{n}}, y_{\hat{n}})\Delta t + \sigma_2 y_{\hat{n}} \Delta B^2_{\hat{n}}, \end{aligned} \tag{3.1}$$

where random variables $\Delta B^i_{\hat{n}}$, $i = 1, 2$, are independent and identically distributed normal random variables with mean zero and variance Δt, and $\hat{n}$ is the number of iterations. Using formulas (3.1), we perform the Monte Carlo simulation for 1000 times to acquire an estimate of the probability density function. The results of the Monte Carlo simulation are displayed in Fig. 3.1(b). We can see that although there are some slight differences between the Monte Carlo results and the numerical simulation results, there is generally a good agreement (see Fig. 3.1(a)). In fact, the main reason for this slight difference is that Monte Carlo simulations must be performed multiple times to obtain relatively accurate statistical information. However, as the number of trials increases, it will lead to a huge amount of computation. Furthermore, due to the discrete nature of the Monte Carlo method, subtle dynamic features may be ignored or discarded as "numerical noise" during numerical integration.

4. Results

The probability density functions of model (2.1) with noise intensity $\sigma = 0.03$ and initial value $(4.1, 4.1)$ at four different times are sketched in Fig. 4.1. The highest probability density is located in the dark red area in Fig. 4.1. At time $T = 1$, the red area is mainly concentrated near the initial value, which indicates that the stochastic trajectory at this time is hovering near the initial point (see Fig. 4.1(a)). However this situation changes at time $T = 5, T = 15$ and $T = 25$, the dark red area gradually moves as time goes on until it reaches near the low biomass state $(1, 1)$ (see Fig. 4.1(b), (c) and (d)), which suggests that stochastic trajectory starting near high biomass state is attracted by low biomass state. This result agrees with the behavior of the previous stochastic trajectory (see Fig. 2.2). It is worthy to remark that by comparing the numerical simulation results, we uncover that the shape of the probability density function does not alter after the time $T = 25$, therefore the system can be treated as stationary.

Next, for a fixed terminal time $T = 25$, the influence of noise intensity on the evolution of the probability density function and the maximal likely trajectories is discussed. Fig. 4.2 shows that the probability density function (the left plots of Fig. 4.2) and corresponding contour plots (the right plots of Fig. 4.2) of stochastic model (2.1) with different values of the noise intensity σ. From top to bottom, as σ increases, the probability density function experiences a process from unimodal to bimodal and then to unimodal again, but the position of the corresponding single peak has altered. In Fig. 4.2(a)–(b), when σ is small, the peak located near the high biomass state is quite high, indicating most of the stochastic trajectories starting from point $(4.1, 4.1)$ are concentrated near the high biomass state. One can see the weaker noise does not affect the dynamics of stochastic model (2.1). As σ increases further, the changes in the two peaks of the stationary probability density function are shown in Fig. 4.2(c)–(f). The peak near the low biomass state becomes higher while the peak corresponding to high biomass state diminishes gradually. When the disturbance intensity surpasses the critical noise intensity where the two peaks have the same height, the low biomass state dominates (see Fig. 4.2(g) and (h)), and thus we can state that the ecosystem experiences a regime shift under Gaussian noise.

For a fixed time t_i, we record the maximum of probability density function $p(x, y, t_i)$ to find the location (x_i, y_i), then we link this series of points $(x_i, y_i), i = 1, 2, \ldots$ to obtain the maximal likely trajectory.

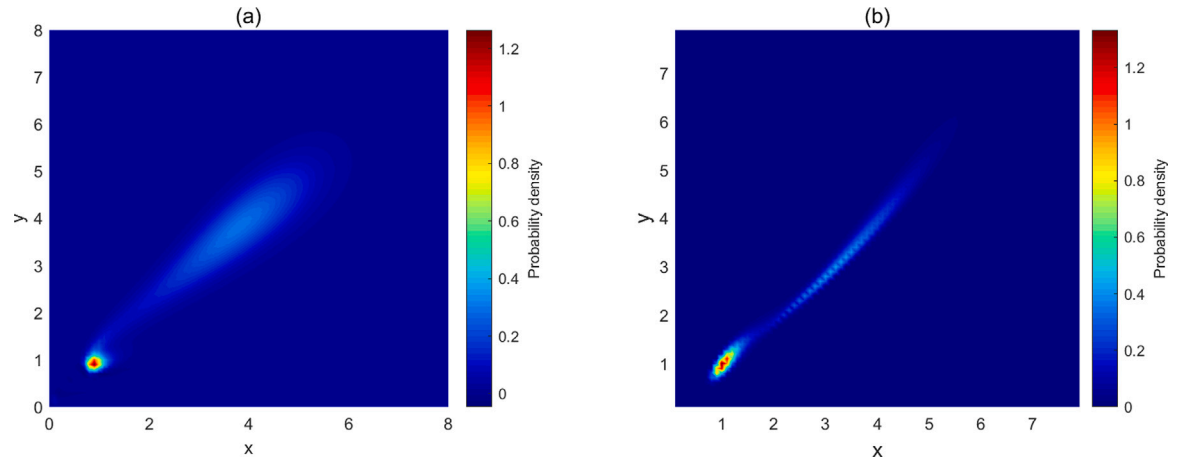

Fig. 3.1. Probability density function $p(x, y)$ of the system (2.1) with $s = 1$ and $\sigma = 0.1$. (a) Numerical solution obtained by the operator-splitting method. (b) Approximate solution obtained by Monte Carlo simulation.

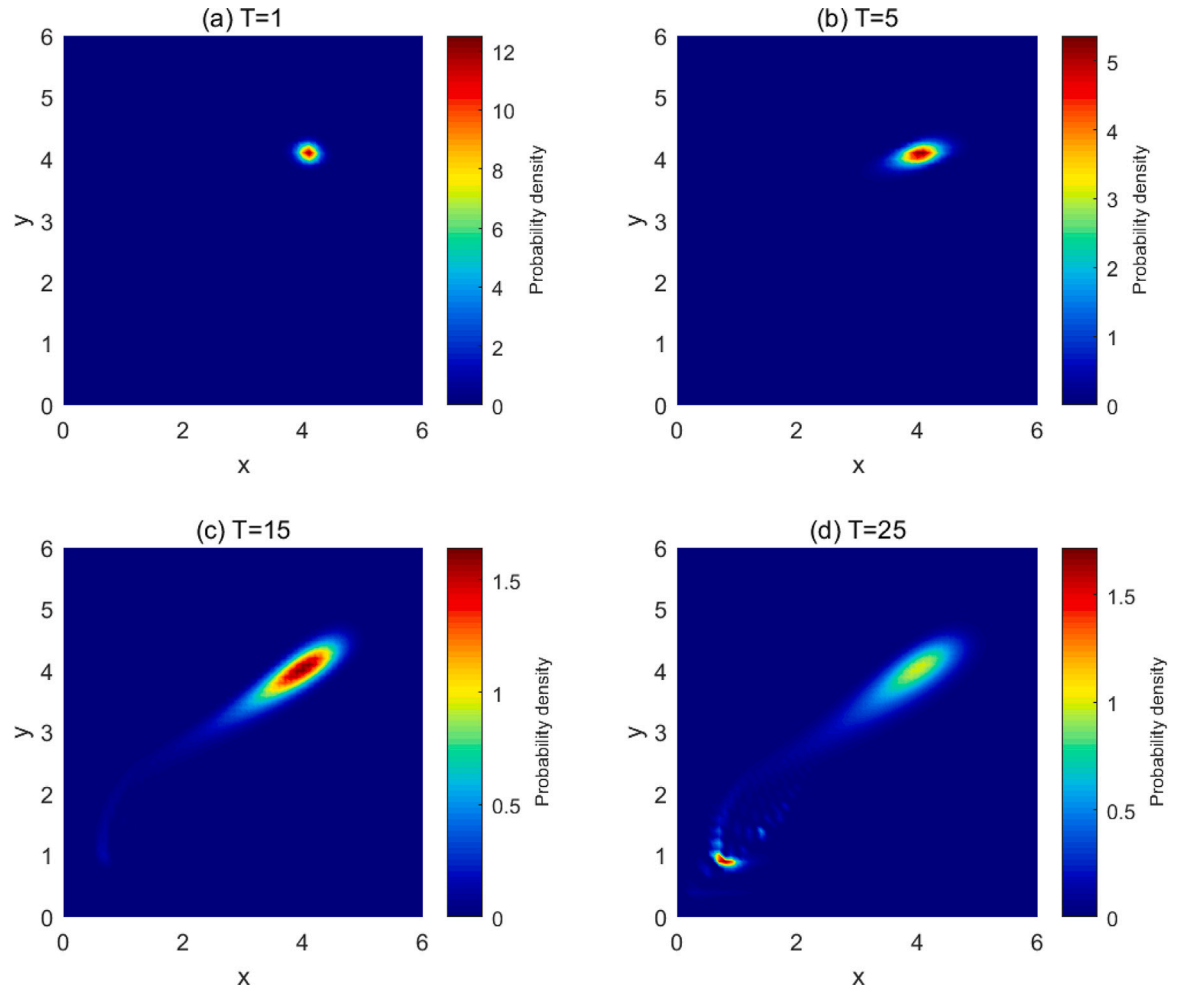

Fig. 4.1. The probability density function of stochastic model (2.1) at different time with $\sigma = 0.03$, $s = 0.5$ and initial value $(4.1, 4.1)$. (a)–(d) shows the representative probability density function images of $T = 1, T = 5, T = 15$, and $T = 25$, respectively. (For interpretation of the references to color in this figure legend, the reader is referred to the web version of this article.)

Through this construction process we clearly see that the "trajectory" is a sequence of locations (x_i, y_i), so it is not the true trajectory of random system (2.1). Note that the prey biomass changes similarly to the predator under the interference of noise. We only present the changes in predator biomass here. The y coordinates of maximal likely trajectory with the same initial value and different noise intensity are presented in Fig. 4.3. In the case of weaker noise intensity ($\sigma = 0.01$ or $\sigma = 0.015$), the time series of predator of the maximal likely trajectories stay around the initial value 4.1 (see the red and blue dashed lines in Fig. 4.3). It can be seen that weaker disturbance events have little effect on the stability of the high biomass state. However, when σ is relatively large ($\sigma = 0.03$ or $\sigma = 0.1$), the maximal likely trajectories

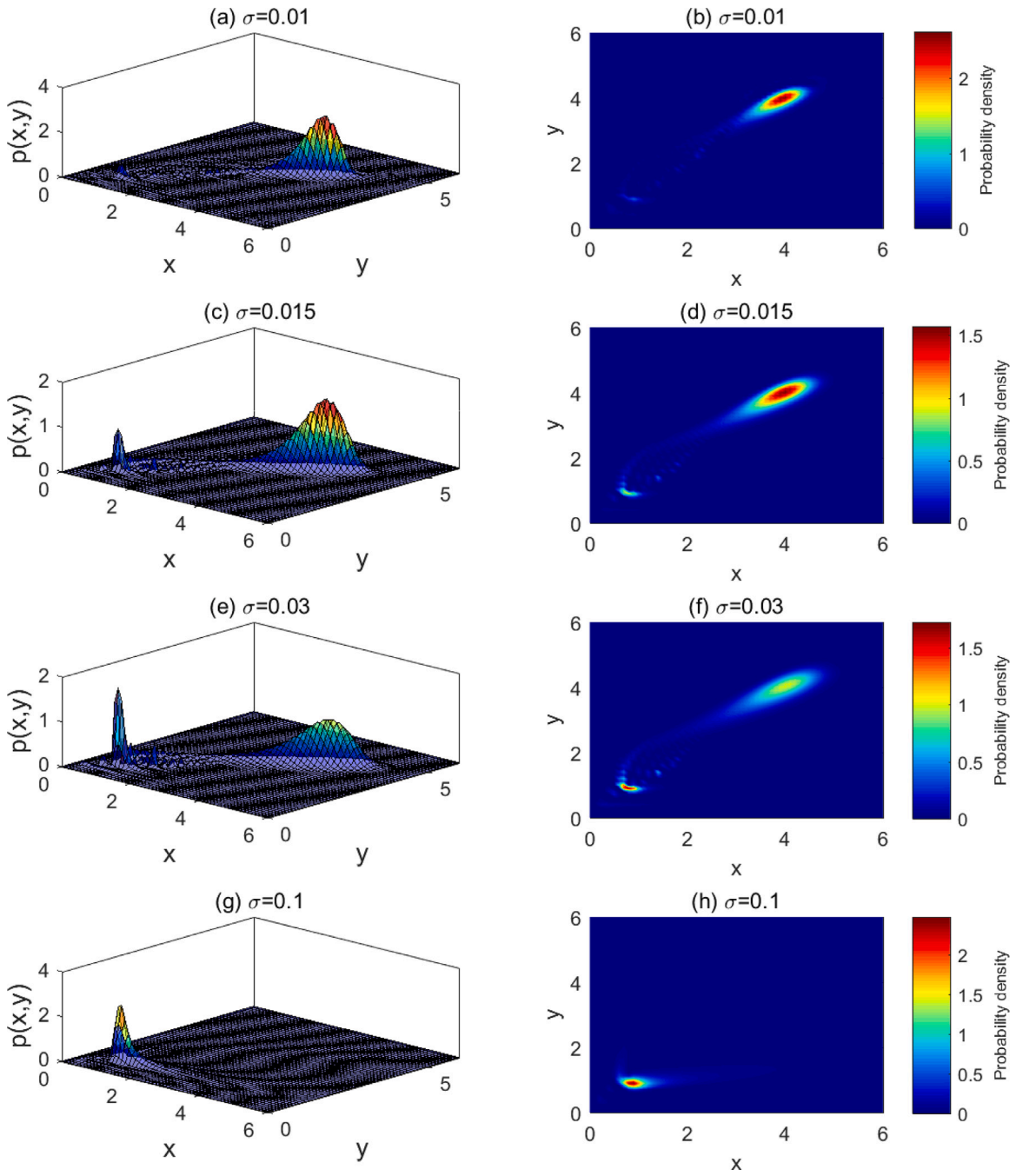

Fig. 4.2. The probability density function (left) and corresponding contour plots (right) of stochastic model (2.1) with initial value $(4.1, 4.1)$ and different σ. The initial value is $(4.1, 4.1)$. Time is limited to 25. From top to bottom, the noise intensity is 0.01, 0.015, 0.03 and 0.1, respectively.

escape from the attraction domain of E_3 and are attracted by E_1. Thus, there must be one intermediate critical value of interference strength σ at which noise-induced tipping occurs. In addition, we can see the vertiginous drop at time $T = 21.86$ (the black solid line) and $T = 6.65$ (the green dashed line) in Fig. 4.3. Fig. 4.4 shows the dependence of the time of abrupt change on the noise intensity σ and the intrinsic growth rate of predator s. Obviously, under increasing noise intensity, the time of abrupt change monotonously decreases, that is, the abrupt change occurs earlier with the stronger noise.

It is worth remarking that for $s \in [0.4, 1.5]$, the position and stability of equilibrium points of deterministic system (2.2) do not change. Our simulation results show that the time of the sudden decline of biomass depends not only on the noise intensity σ but also on the intrinsic growth rate of predator s. In the following, therefore, we take the intrinsic growth rate s to be a control parameter for investigating the effect of s on the time of abrupt change. As shown in Fig. 4.4, for $s = 0.4, 0.5, 1.0$, and 1.5, we reveal that all four curves decrease with the increase of noise intensity. When the disturbance event is strong enough, the tipping time is insensitive to changes in s.

For an ecosystem with alternative stable states, the pressure from the drivers of environmental conditions forces the system closer to a tipping point. Once environmental conditions cross the tipping point, the system undergoes a critical transition and transitions to a distinct state. The term “tipping point” here generally refers to a critical threshold at which a tiny perturbation can qualitatively alter the state or development of a system. From the definitions of these three common tipping mechanisms in the introduction, it can be seen that for B-tipping, N-tipping, and R-tipping, the “tipping point” refers to a bifurcation

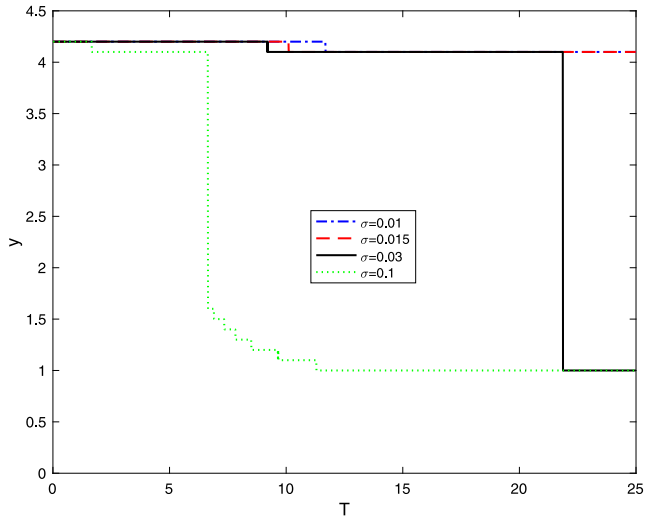

Fig. 4.3. The time variation of the y-coordinate of the maximal likely trajectories with initial value (4.1, 4.1) and different noise intensity σ. (For interpretation of the references to color in this figure legend, the reader is referred to the web version of this article.)

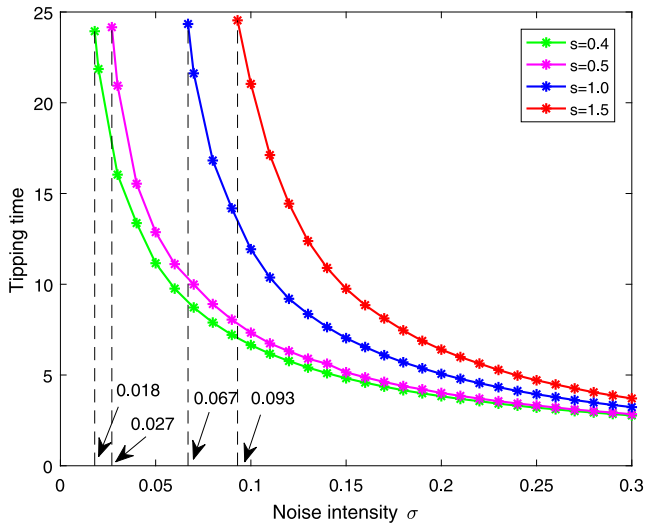

Fig. 4.4. The time for abrupt change as function of noise intensity for stochastic model (2.1) with initial value (4.1, 4.1) and different values of parameter s. (For interpretation of the references to color in this figure legend, the reader is referred to the web version of this article.)

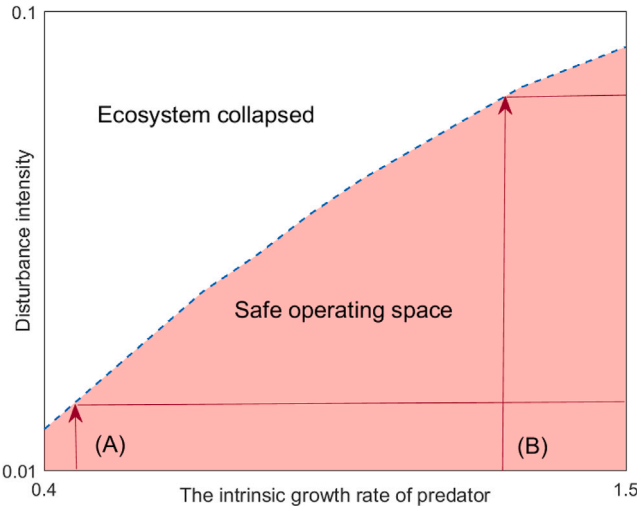

Fig. 4.5. Safe Operating Set (SOS) for the population ecosystem. A predator growth rate that is currently at a safe level (A) needs to be adjusted to a higher value (B) to ensure system (2.1) within the safe operating set in a strongly disturbed event.

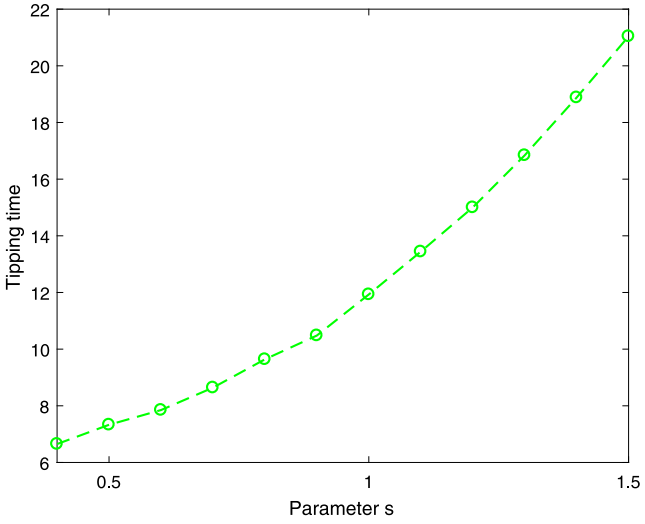

Fig. 4.6. Dependence of the tipping time on the parameter s.

point, a critical noise intensity, and a critical rate of change in system parameter, respectively. In this paper, we consider the noise-induced tipping mechanism, so it is natural to shift our attention to critical noise intensity. Aiming at determining the smallest value of noise intensity (tipping point) that incurs a critical transition from the high biomass state to the low biomass state, we draw vertical lines in Fig. 4.4 from the highest point of the four curves. The critical noise intensities are approximately $\widetilde{\sigma} = 0.018, 0.027, 0.067$, and 0.093 for growth rates $s = 0.4, 0.5, 1.0$, and 1.5, respectively. For $s \in [0.4, 1.5]$, the dotted line in Fig. 4.5 shows the relationship between intrinsic growth rate s and the critical noise intensity $\widetilde{\sigma}$. Our simulations indicate that the minimum external force required for the critical transition increases as the rate of predator growth increases. Meanwhile, the dotted line also divides the $\sigma - s$ parameter space into two parts including the ecosystem collapsed and the safe operating set (SOS) in which system state remains near high biomass. If the multiple environmental drivers (e.g., extreme weather events, fires and floods) trigger the system parameters crossed the bound, the system will undergo a transition to an alternative state (the low biomass state). As Fig. 4.5 illustrates, therefore, a predator growth rate that is currently at a safe level (A) needs to be adjusted to a higher value (B) to ensure system (2.1) within the safe operating set in a strongly disturbed event. The SOS illustrates opportunities to manage habitat quality or harvest to maintain ecosystem biodiversity in the presence of uncertainties such as extreme climates condition, human behavior, etc.

Another observation shown in Fig. 4.6 is that for a fixed noise intensity (here, we take $\sigma = 0.1$), the greater the growth rate of predators, the longer it takes for the maximal possible trajectory to shift to the regime of low biomass. The above simulation results related to tipping time show that increasing the intensity of external disturbance events accelerates the reduction of biomass in the ecosystem. For a fixed intensity of disturbance event, the increase of predator growth rate has a positive effect on promoting stability of high biomass state. It should be emphasized that the word "stability" here is determined according to the magnitude of the tipping time. Generally, we think that the larger the value of tipping time, the greater the ability of the system to maintain high biomass and the stronger the stability of the equilibrium point.

Next, in order to verify the validity of the metric (tipping time) proposed above, we shall explore the influence of parameter s on the stability of equilibrium point E_3 from the perspective of quasi-potentials. For a gradient system with multiple stable states, ball-in-cup diagram is a convenient method to visualize states in corresponding stochastic system [37]. In the ball-in-cup diagram, the state of the system can be imagined as the position of a ball rolling on a surface which is defined by a potential function. The ball constantly rolls downhill on the surface and eventually falls into a valley (the local minimum of the potential function). These valleys correspond to the stable state of the system and the peaks to the unstable state. Environmental random forces can propel the ball from one attraction domain over a mountain to another. Therefore, the potential function can provide an effective method to compare the stability of different stable states by the depth difference of the valley (the potential depth) [33,38]. However, usually only one-dimensional or gradient systems can write down a potential function. For non-gradient systems, [33,39,40] proposed the quasi-potential as a way similar to the traditional potential function to quantify the difficulty of moving the system state from one domain of attraction to another.

Mathematically, we assume that $\theta(t)$ is a path, starting from a stable state $\theta(0) = E_*$ to another state $\theta(T) = x$. T is the total time the system spends along this path. According to the Freidlin–Wentzell theory of large deviations [41], the amount of work required for the state of the system to trace a candidate path can be quantified by a functional S_T named the action, one can see Ref. [41] for more details. Then, the quasi-potential is defined as the value of the action S_T for the minimum-action path between E_* and x, denoted

$$H_{E_*}(x) = \inf_{T>0}\{S_T(\theta)|\theta(0) = E_*, \theta(T) = x\}. \tag{4.1}$$

Since the calculation of the quasi-potential involves a class of static Hamilton–Jacobi equations, the standard finite element and finite difference methods are often infeasible. Fortunately, Sethian et al. proposed a family of fast ordered upwind methods to approximate solutions to this class of equations [42,43]. Subsequently, Cameron [40] improved the standard ordered headwind method. Based on Cameron's algorithm, Moore et al. [44] developed a freely available R package $QPot$ that computes quasi-potentials efficiently.

In this paper, resorting to the R package $QPot$, the quasi-potential H of model (2.1) is derived, illustrated in Fig. 4.7. The quasi-potential at the unstable equilibrium E_2 are 0.0008068, 0.006627 and 0.01619 for $s = 0.5$, $s = 1.0$ and $s = 1.5$, respectively. The quasi-potential at equilibrium points E_3 and E_1 are $1.62 * 10^{-5}$ and $3.02 * 10^{-6}$ respectively for all parameters s. Then, we can easily calculate that the quasi-potential depth at equilibrium point $E_3(E_1)$ are $\Delta H_1 = 0.0007905(0.00080378)$, $\Delta H_2 = 0.006611(0.00662398)$ and $\Delta H_3 = 0.016173(0.01618698)$ for $s = 0.5$, $s = 1.0$ and $s = 1.5$, respectively. It is obvious that as the growth rate of the predator increases, the valley at the equilibrium point E_3 is deeper, which indicates that the stability of E_3 is stronger. Thus, more random force is needed to push a ball from the basin of attraction of E_3 to that of E_1. We can see that the result of the stability of equilibrium point E_3 from the metric of quasi-potential has a good agreement with the result obtained from the analysis of tipping time in Fig. 4.6.

5. Discussion

In recent years, the construction of ecological civilization and sustainable development have been elevated to a national strategic position. In the theoretical and practical studies of ecosystem degradation and restoration, more and more researchers have paid extensive attention to the phenomenon of abrupt change in multi-steady state ecosystems [3,45]. In general, such dramatic changes have potentially negative impacts on ecosystem persistence and human well-being. It is therefore necessary to formulate strategies to adapt, mitigate and avoid such changes. In this paper, we develop a Leslie-type predator–prey model with environmental stochasticity that is suddenly forced through population collapse, in the presence of strong environmental noise. To reveal the mechanism underlying the abrupt transition in population size, we have put forward a research framework, based on transition probability densities and FPK equation, to gain the maximal likely trajectory from high biomass state to low biomass state under Gaussian white noise. Subsequently, we acquire the tipping time of population collapse and the critical noise intensity inducing the state transition by using the maximal likely trajectory.

In light of the results of numerical experiments, we uncover that the tipping times of population collapse depend strongly on the noise intensity σ, and the predator growth rate s. For a fixed growth rate of predator, the tipping time of population collapse decreases with the increase of environmental noise intensity (see Fig. 4.4). This shows that environmental disturbance events (such as floods, fires, earthquakes, etc.) can accelerate the collapse of the ecosystem. On the other hand, for a fixed noise intensity, we observe that increasing the growth rate of predators would effectively prolong the time the system was maintained in a high biomass state (see Fig. 4.6). In other words, an increase in the growth rate of predators is conducive to the stability and biodiversity of the ecosystem from the perspective of a longer tipping time. To verify this conclusion, we also calculate the quasi-potentials of the corresponding equilibrium state for different predator growth rates. We can see that the result of the stability of high biomass state from the metric of quasi-potential has a good agreement with the result obtained from the analysis of tipping time. The SOS of an ecosystem–the range of conditions that maintain population size at relatively high levels–depends on various factors including environmental randomness and habitat quality (which determines predator growth rates). The curve in Fig. 4.5 explains compensatory interactions. To maintain biomass within the SOS, predator growth rates must be upregulated with increasing environmental disturbance.

For a purely stochastic transition event, since there is no effective early warning indicator, calculating the most likely trajectory from one state to another is an effective tool for understanding the mechanism of sudden transition in a population ecosystem. Our study in this paper provides a probabilistic framework for investigating the mechanisms underlying ecosystem collapse under the influence of environmental disturbances. In addition, our method here has two obvious advantages for obtaining the most likely transition orbits. First, we numerically solve the corresponding Fokker–Planck equation to acquire the probability density of the transition path, thus avoiding the difficulty of obtaining the action functional in the Onsager–Machlup method [46,47]. Second, our method here is not an asymptotic approach and thus avoids the assumption that the noise intensity is sufficiently small in the large deviation theory [41].

At present, there has been some excellent work on the tipping phenomenon in the predator–prey model. For example, Alkhayuon et al. [48] identified a new mechanism called phase-sensitive tipping, where tipping to extinction occurs only from certain phases of the cycle. Vanselow et al. [14] found that the Rosenzweig–MacArthur predator–prey model can undergo a rate-induced critical transition in response to continued decline in habitat quality, leading to ecosystem collapse. However, in our work we pay our attention to noise-induced tipping. It is worth noting that none of these tipping mechanisms involve any bifurcation and all these works focus on one tipping mechanism. In nature, there can be multiple tipping mechanisms working together, and one of them is dominant [49]. It is an interesting research direction to explore the results of the joint action of multiple tipping mechanisms [50]. Also, in contrast to [48] that focused on the transition phenomenon from limit cycle to equilibrium, we focus on shifting from one equilibrium to another. In fact, the transition of population size from a stationary state to a periodically oscillating state is quite common in nature. We will devote to developing suitable early warning signals to predict the onset of oscillations in future work.

Although the example we study in this paper is about a two-dimensional population dynamics model, our research ideas can be

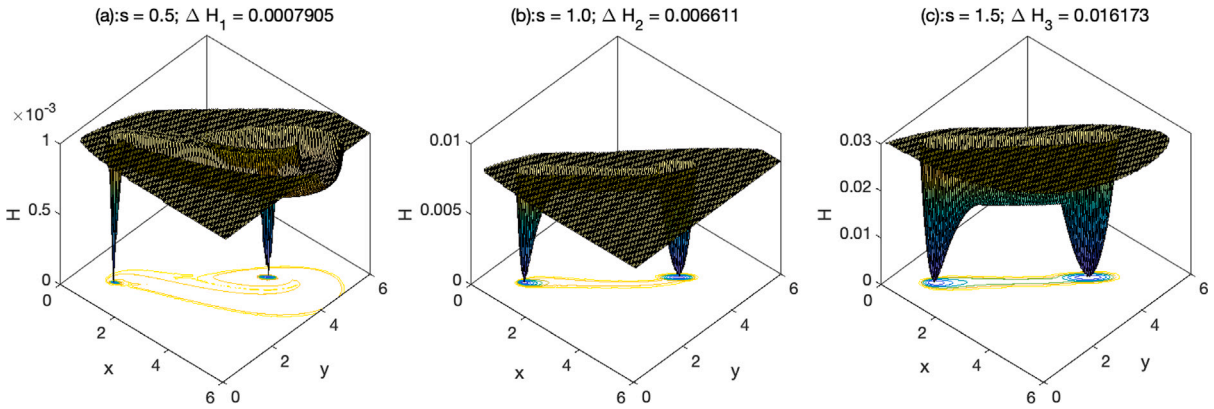

Fig. 4.7. The quasi-potential function for stochastic system (2.1) with fixed noise intensity $\sigma = 0.001$ and different intrinsic growth rate of predator s. The quasi-potential depth of equilibrium point E_3 are: (a) $\Delta H_1 = 0.0007905$, (b) $\Delta H_2 = 0.006611$ and (c) $\Delta H_3 = 0.016173$, respectively.

easily extended to higher-dimensional systems. For example, for a three-dimensional Itô stochastic differential equation, we can obtain the corresponding FPK equation for the evolution of the transition probability density, which can also be solved using the operator splitting method. We have noticed the literature [51] where by applying the path integral formalism and the saddle point approximation, the authors reduce the high-dimensional stochastic neural network model to a two-dimensional system and describes numerically and analytically how parameters and stochasticity affect the dynamics of the system. We believe that for systems in more than three dimensions, the methods implemented in literature [51,52] are potential tools for studying the most likely transition paths.

CRediT authorship contribution statement

Anji Yang: Conceptualization, Investigation, Writing – original draft. **Hao Wang:** Conceptualization, Investigation, Writing – review & editing. **Sanling Yuan:** Conceptualization, Investigation, Writing – review & editing, Supervision.

Declaration of competing interest

The authors declare that they have no known competing financial interests or personal relationships that could have appeared to influence the work reported in this paper.

Data availability

No data was used for the research described in the article.

Acknowledgments

SY's research is partially supported by National Natural Science Foundation of China (No. 12071293) and Natural Science Foundation of Shanghai (No. 23ZR1445100). HW's research is partially supported by Natural Sciences and Engineering Research Council of Canada (Individual Discovery Grant RGPIN-2020-03911 and Discovery Accelerator Supplement Award RGPAS-2020-00090).

Appendix A. Holling type functional response functions

The functional response function $p(x)$, which depicts the change in the density of the prey attacked per unit time per predator as the prey density changes, is a key factor in modeling the ecological interaction between predators and their prey and plays an important role in determining the dynamics of the model. There are many type functional response functions appeared in literatures, and in particular the following three Holling type functional response functions are most often used [53]:

- Holling type I, i.e., $p(x) = mx(m > 0)$. This type is usually applied to algae, cells, and lower organisms.
- Holling type II, i.e., $p(x) = \frac{mx}{a+x}(m > 0, a > 0)$. It is usually applied to invertebrates.
- Holling type III, i.e., $p(x) = \frac{mx^2}{ax^2+1}(m > 0, a > 0)$. This type is generally applied to vertebrates [54].

In [34,35], the authors used a more generalized form of Holling type III response function as follows:

$$p(x) = \frac{mx^2}{ax^2 + bx + 1}, \tag{A.1}$$

where $m > 0, a > 0$ and b is a constant number. This generalized type of Holling III functional response function suggests that predators have some form of learning behavior, specifically, when the prey biomass is below a certain threshold, predators will not exploit prey as food with any large intensity and converges to $\frac{m}{a}$ as the prey biomass tends to infinity. But for $b \geq 0$, we can see from Fig. A.1(a) that once this density threshold is exceeded, predators increase their predation rate to its saturation level $\frac{m}{a}$ monotonically; while for $b < 0$, we can see from Fig. A.1(b) that predation rate increases first to a maximum and then drops, and converges to $\frac{m}{a}$ as the prey biomass tends to infinity. In the case of $b < 0$, model (2.2) can exhibit complex dynamics such as the bistability between multiple attractors.

Appendix B. Detailed numerical method to gain the probability density function

For two-dimension Itô's stochastic differential Eq. (2.1), the corresponding Fokker–Planck (FPK) equation is

$$\begin{aligned}\frac{\partial p(x,y,t)}{\partial t} = &-\frac{\partial(f_1 p(x,y,t))}{\partial x} + \frac{1}{2}\frac{\partial^2(g_1 p(x,y,t))}{\partial x^2} \\ &- \frac{\partial(f_2 p(x,y,t))}{\partial y} + \frac{1}{2}\frac{\partial^2(g_2 p(x,y,t))}{\partial y^2},\end{aligned} \tag{B.1}$$

with a delta initial condition $p(x, y, 0) = \delta(x - x_0, y - y_0)$, where

$$\begin{aligned} f_1 &= rx\left(1 - \frac{x}{K}\right) - \frac{mx^2 y}{ax^2 + bx + 1}, \quad g_1 = (\sigma_1 x)^2, \\ f_2 &= sy\left(1 - \frac{y}{hx}\right), \quad g_2 = (\sigma_2 y)^2. \end{aligned} \tag{B.2}$$

In the following, we numerically solve Eq. (B.1) on the rectangular bounded domain $D = (0, L) \times (0, L)$ with the boundary condition

$$p(x, y, t) = 0, \qquad \text{for } (x(t), y(t)) \in \partial D, \tag{B.3}$$

where ∂D is the boundary surface.

We employ an operator-splitting method [55–58] for FPK Eq. (B.1) and divide the two-dimensional spatial operators into the following 2

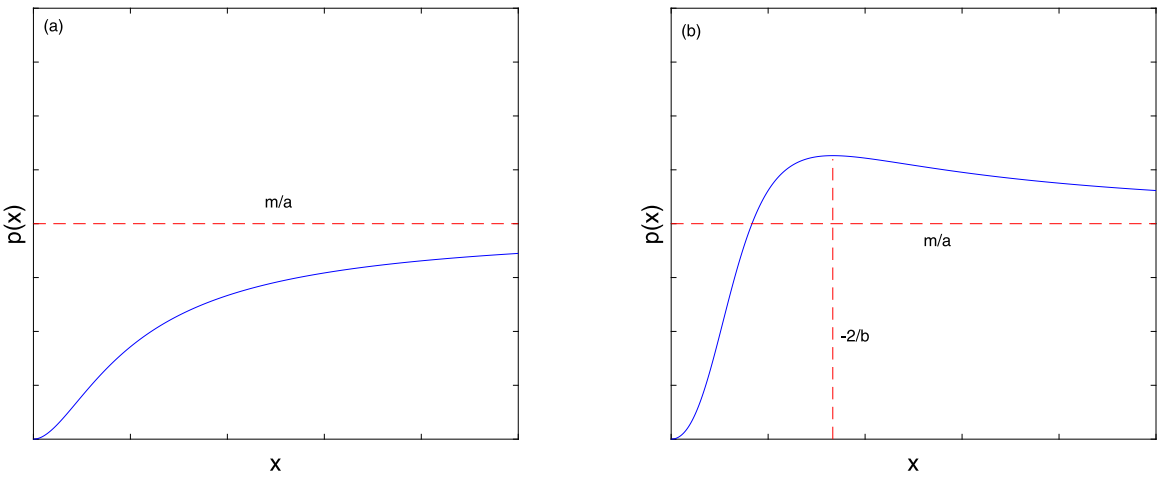

Fig. A.1. Generalized Holling III functional response. (a) $b \geq 0$; (b) $b < 0$.

one-dimensional operators:

$$\frac{p^{m+1/2}-p^m}{\Delta t} = -\frac{\partial}{\partial x}\left(f_1\frac{p^{m+1/2}+p^m}{2}\right) + \frac{1}{2}\frac{\partial^2}{\partial x^2}\left(g_1\frac{p^{m+1/2}+p^m}{2}\right), \quad \text{(B.4)}$$

and

$$\frac{p^{m+1}-p^{m+1/2}}{\Delta t} = -\frac{\partial}{\partial y}\left(f_2\frac{p^{m+1}+p^{m+1/2}}{2}\right) + \frac{1}{2}\frac{\partial^2}{\partial y^2}\left(g_2\frac{p^{m+1}+p^{m+1/2}}{2}\right), \quad \text{(B.5)}$$

where $p^m, p^{m+1/2}$ and p^{m+1} represent the values of the probability density function $p(x,y,t)$ at time $m\Delta t, (m+1/2)\Delta t$ and $(m+1)\Delta t$, respectively. Let us discretize the spatial domain $D = (0,6)\times(0,6)$ as $x_1 = 0, x_2 = \Delta x, \ldots, x_N = 6$ and $y_1 = 0, y_2 = \Delta y, \ldots, y_N = 6$, where

$$\Delta x = \frac{x_N - x_1}{N-1}, \qquad \Delta y = \frac{y_N - y_1}{N-1}$$

and N is taken as 61. We take the time step size $\Delta t = 0.01$. $p_{i,j}$ denote the numerical solution of p at (x_i, y_j, t). The finite differences are used implicitly to Eq. (B.4)

$$\begin{aligned}&\frac{p_{i,j}^{m+1/2}-p_{i,j}^m}{\Delta t} = \\ &-\frac{1}{2}\frac{f_{1,i+1,j}p_{i+1,j}^{m+1/2} - f_{1,i-1,j}p_{i-1,j}^{m+1/2} + f_{1,i+1,j}p_{i+1,j}^m - f_{1,i-1,j}p_{i-1,j}^m}{2\Delta x} \\ &+\frac{1}{4}\frac{g_{1,i+1,j}p_{i+1,j}^{m+1/2} - 2g_{1,i,j}p_{i,j}^{m+1/2} + g_{1,i-1,j}p_{i-1,j}^{m+1/2} + g_{1,i+1,j}p_{i+1,j}^m - 2g_{1,i,j}p_{i,j}^m + g_{1,i-1,j}p_{i-1,j}^m}{(\Delta x)^2},\end{aligned} \quad \text{(B.6)}$$

where $i,j = 1,2,\ldots,N-1$ and $m = 0,1,2,\ldots$. The terms related to the time levels $m+1/2$ and m in Eq. (B.6) are respectively moved to the left and right sides of the equal sign, and we let $u_1 = \frac{\Delta t}{\Delta x}$, $v_1 = \frac{\Delta t}{(\Delta x)^2}$, $\alpha_i = -\frac{u_1 f_{1,i-1}}{4} - \frac{v_1 g_{1,i-1}}{4}$, $\beta_i = 1 + \frac{v_1 g_{1,i}}{2}$, $\gamma_i = \frac{u_1 f_{1,i+1}}{4} - \frac{v_1 g_{1,i+1}}{4}$ and $\eta_i = 1 - \frac{v_1 g_{1,i}}{2}$. Then, Eq. (B.6) becomes

$$\alpha_i p_{i-1,j}^{m+1/2} + \beta_i p_{i,j}^{m+1/2} + \gamma_i p_{i+1,j}^{m+1/2} = -\alpha_i p_{i-1,j}^m + \eta_i p_{i,j}^m - \gamma_i p_{i+1,j}^m. \quad \text{(B.7)}$$

We can omit the subscript j since it does not affect the partial derivatives of x. Letting $\delta_i = -\alpha_i p_{i-1}^m + \eta_i p_i^m - \gamma_i p_{i+1}^m$ we have

$$\alpha_i p_{i-1}^{m+1/2} + \beta_i p_i^{m+1/2} + \gamma_i p_{i+1}^{m+1/2} = \delta_i. \quad \text{(B.8)}$$

Eq. (B.8) can be written in matrix form as follows:

$$Ap = \delta, \quad \text{(B.9)}$$

with $p = \left(p_1^{m+1/2}, p_2^{m+1/2}, \ldots, p_n^{m+1/2}\right)^T$, $\delta = \left(\delta_1, \delta_2, \ldots, \delta_n\right)^T$ and

$$A = \begin{bmatrix} \beta_1 & \gamma_1 & 0 & \cdots & 0 & 0 & 0 \\ \alpha_2 & \beta_2 & \gamma_2 & \cdots & 0 & 0 & 0 \\ 0 & \alpha_3 & \beta_3 & \cdots & 0 & 0 & 0 \\ \cdots & \cdots & \cdots & \cdots & \cdots & \cdots & \cdots \\ 0 & 0 & 0 & \cdots & \alpha_{n-1} & \beta_{n-1} & \gamma_{n-1} \\ 0 & 0 & 0 & \cdots & 0 & \alpha_n & \beta_n \end{bmatrix}.$$

Obviously, the coefficient matrix A is tridiagonal. After gaining the probability density at the time level m, it is easy to acquire the solution of the time level $m+1/2$ by using the chasing method [59] for the tridiagonal Eqs. (B.9) as follows:

$$p = A^{-1}\delta.$$

Similarly, in terms of finite differences methods, Eq. (B.5) becomes

$$\begin{aligned}&\frac{p_j^{m+1}-p_j^{m+1/2}}{\Delta t} = \\ &-\frac{1}{2}\frac{f_{2,j+1}p_{j+1}^{m+1} - f_{2,j-1}p_{j-1}^{m+1} + f_{2,j+1}p_{j+1}^{m+1/2} - f_{2,j-1}p_{j-1}^{m+1/2}}{2\Delta y} \\ &+\frac{1}{4}\frac{g_{2,j+1}p_{j+1}^{m+1} - 2g_{2,j}p_j^{m+1} + g_{2,j-1}p_{j-1}^{m+1} + g_{2,j+1}p_{j+1}^{m+1/2} - 2g_{2,j}p_j^{m+1/2} + g_{2,j-1}p_{j-1}^{m+1/2}}{(\Delta y)^2}.\end{aligned} \quad \text{(B.10)}$$

By letting $u_2 = \frac{\Delta t}{\Delta y}$, $v_2 = \frac{\Delta t}{(\Delta y)^2}$, $\alpha_j = -\frac{u_2 f_{2,j-1}}{4} - \frac{v_2 g_{2,j-1}}{4}$, $\beta_j = 1 + \frac{v_2 g_{2,j}}{2}$, $\gamma_j = \frac{u_2 f_{2,j+1}}{4} - \frac{v_2 g_{2,j+1}}{4}$ and $\eta_j = 1 - \frac{v_2 g_{2,j}}{2}$, Eq. (B.10) is rewritten as

$$\alpha_j p_{j-1}^{m+1} + \beta_j p_j^{m+1} + \gamma_j p_{j+1}^{m+1} = \delta_j, \quad \text{(B.11)}$$

where $\delta_j = -\alpha_j p_{j-1}^{m+1/2} + \eta_j p_j^{m+1/2} - \gamma_j p_{j+1}^{m+1/2}$. Here we resort to the chasing method to acquire the transition probability density at the time level $m+1$. When t is sufficiently large, we gain the stationary probability density function $p(x,y)$. The whole program takes about 2 min using MatLab R2019a running under macOS on a 1.6 GHz Intel Core i5.

References

[1] Clements CF, Ozgul A. Indicators of transitions in biological systems. Ecol Lett 2018;21(6):905–19. http://dx.doi.org/10.1111/ele.12948.
[2] Bauch CT, Sigdel R, Pharaon J, Anand M. Early warning signals of regime shifts in coupled human–environment systems. Proc Natl Acad Sci USA 2016;113(51):14560–7. http://dx.doi.org/10.1073/pnas.1604978113.
[3] Ratajczak Z, Carpenter SR, Ives AR, Kucharik CJ, Ramiadantsoa T, Stegner MA, et al. Abrupt change in ecological systems: Inference and diagnosis. Trends Ecol Evol 2018;33(7):513–26. http://dx.doi.org/10.1016/j.tree.2018.04.013.
[4] Scheffer M, Carpenter SR. Catastrophic regime shifts in ecosystems: Linking theory to observation. Trends Ecol Evol 2003;18(12):648–56. http://dx.doi.org/10.1016/j.tree.2003.09.002.

[5] Drake JM, Griffen BD. Early warning signals of extinction in deteriorating environments. Nature 2010;467(7314):456–9. http://dx.doi.org/10.1038/nature09389.

[6] Pinsky ML, Jensen OP, Ricard D, Palumbi SR. Unexpected patterns of fisheries collapse in the world's oceans. Proc Natl Acad Sci USA 2011;108(20):8317–22. http://dx.doi.org/10.2307/25830048.

[7] Daskin JH, Stalmans M, Pringle RM. Ecological legacies of civil war: 35-year increase in savanna tree cover following wholesale large-mammal declines. J Ecol 2016;104(1):79–89. http://dx.doi.org/10.1111/1365-2745.12483.

[8] Plagányi ÉE, Ellis N, Blamey LK, Morello EB, Norman-Lopez A, Robinson W, et al. Ecosystem modelling provides clues to understanding ecological tipping points. Mar Ecol Prog Ser 2014;512:99–113. http://dx.doi.org/10.3354/meps10909.

[9] Lesk C, Rowhani P, Ramankutty N. Influence of extreme weather disasters on global crop production. Nature 2016;529(7584):84–7. http://dx.doi.org/10.1038/nature16467.

[10] Ashwin P, Wieczorek S, Vitolo R, Cox P. Tipping points in open systems: Bifurcation, noise-induced and rate-dependent examples in the climate system. Philos T R Soc A 2012;370(1962):1166–84. http://dx.doi.org/10.1098/rsta.2011.0306.

[11] Kuehn C. A mathematical framework for critical transitions: Bifurcations, fast–slow systems and stochastic dynamics. Physica D 2011;240(12):1020–35. http://dx.doi.org/10.1016/j.physd.2011.02.012.

[12] Scheffer M, Bascompte J, Brock WA, Brovkin V, Carpenter SR, Dakos V, et al. Early-warning signals for critical transitions. Nature 2009;461(7260):53–9. http://dx.doi.org/10.1038/nature08227.

[13] Kuehn C. A mathematical framework for critical transitions: Normal forms, variance and applications. J Nonlinear Sci 2013;23(3):457–510. http://dx.doi.org/10.1007/s00332-012-9158-x.

[14] Vanselow A, Wieczorek S, Feudel U. When very slow is too fast-collapse of a predator-prey system. J Theoret Biol 2019;479:64–72. http://dx.doi.org/10.1016/j.jtbi.2019.07.008.

[15] Siteur K, Eppinga MB, Doelman A, Siero E, Rietkerk M. Ecosystems off track: Rate-induced critical transitions in ecological models. Oikos 2016;125(12):1689–99. http://dx.doi.org/10.1111/oik.03112.

[16] Boettiger C. From noise to knowledge: How randomness generates novel phenomena and reveals information. Ecol Lett 2018;21(8):1255–67. http://dx.doi.org/10.1111/ele.13085.

[17] Horsthemke W. Noise induced transitions. In: Non-equilibrium dynamics in chemical systems. Springer; 1984, p. 150–60. http://dx.doi.org/10.1007/978-3-642-70196-2_23.

[18] Forgoston E, Moore RO. A primer on noise-induced transitions in applied dynamical systems. SIAM Rev 2018;60(4):969–1009. http://dx.doi.org/10.1137/17m1142028.

[19] Hou J, Ma H, He D, Sun J, Nie Q, Lin W. Harvesting random embedding for high-frequency change-point detection in temporal complex systems. Natl Sci Rev 2022;9(4):nwab228. http://dx.doi.org/10.1093/nsr/nwab228.

[20] Patel D, Ott E. Using machine learning to anticipate tipping points and extrapolate to post-tipping dynamics of non-stationary dynamical systems. Chaos 2023;33(2):023143. http://dx.doi.org/10.1063/5.0131787.

[21] Carpenter SR, Arani BM, Hanson PC, Scheffer M, Stanley EH, Van Nes E. Stochastic dynamics of Cyanobacteria in long-term high-frequency observations of a eutrophic lake. Limnol Oceanogr Lett 2020;5(5):331–6. http://dx.doi.org/10.1002/lol2.10152.

[22] Blasius B, Rudolf L, Weithoff G, Gaedke U, Fussmann GF. Long-term cyclic persistence in an experimental predator–prey system. Nature 2020;577(7789):226–30. http://dx.doi.org/10.1038/s41586-019-1857-0.

[23] Dakos V, Carpenter SR, Brock WA, Ellison AM, Guttal V, Ives AR, et al. Methods for detecting early warnings of critical transitions in time series illustrated using simulated ecological data. PLoS One 2012;7(7):e41010. http://dx.doi.org/10.1371/journal.pone.0041010.

[24] Boettiger C, Hastings A. No early warning signals for stochastic transitions: Insights from large deviation theory. P Roy Soc B-Biol Sci 2013;280(1766):20131372. http://dx.doi.org/10.1098/rspb.2013.1372.

[25] Carpenter S, Brock W. Early warnings of unknown nonlinear shifts: A nonparametric approach. Ecology 2011;92(12):2196–201. http://dx.doi.org/10.1890/11-0716.1.

[26] Ives AR, Dakos V. Detecting dynamical changes in nonlinear time series using locally linear state-space models. Ecosphere 2012;3(6):1–15. http://dx.doi.org/10.1890/ES11-00347.1.

[27] Duan J. An introduction to stochastic dynamics, Vol. 51. Cambridge University Press; 2015.

[28] Zheng Y, Yang F, Duan J, Sun X, Fu L, Kurths J. The maximum likelihood climate change for global warming under the influence of greenhouse effect and Lévy noise. Chaos 2020;30(1):013132. http://dx.doi.org/10.1063/1.5129003.

[29] Yang F, Sun X, Duan J. On the abrupt change of the maximum likelihood state in a simplified stochastic thermohaline circulation system. Chaos 2021;31(2):021103. http://dx.doi.org/10.1063/5.0037083.

[30] Yang F, Zheng Y, Duan J, Fu L, Wiggins S. The tipping times in an Arctic sea ice system under influence of extreme events. Chaos 2020;30(6):063125. http://dx.doi.org/10.1063/5.0006626.

[31] Cheng X, Wang H, Wang X, Duan J, Li X. Most probable transition pathways and maximal likely trajectories in a genetic regulatory system. Physica A 2019;531:121779. http://dx.doi.org/10.1016/j.physa.2019.121779.

[32] Chen X, Wu F, Duan J, Kurths J, Li X. Most probable dynamics of a genetic regulatory network under stable Lévy noise. Appl Math Comput 2019;348:425–36. http://dx.doi.org/10.1016/j.amc.2018.12.005.

[33] Nolting BC, Abbott KC. Balls, cups, and quasi-potentials: Quantifying stability in stochastic systems. Ecology 2016;97(4):850–64. http://dx.doi.org/10.1890/15-1047.1.

[34] Huang J, Ruan S, Song J. Bifurcations in a predator–prey system of Leslie type with generalized Holling type III functional response. J Differential Equations 2014;257(6):1721–52. http://dx.doi.org/10.1016/j.jde.2014.04.024.

[35] Dai Y, Zhao Y, Sang B. Four limit cycles in a predator–prey system of Leslie type with generalized Holling type III functional response. Nonlinear Anal Real 2019;50:218–39. http://dx.doi.org/10.1016/j.nonrwa.2019.04.003.

[36] Higgins K, Hastings A, Sarvela JN, Botsford LW. Stochastic dynamics and deterministic skeletons: Population behavior of Dungeness crab. Science 1997;276(5317):1431–5. http://dx.doi.org/10.1126/science.276.5317.1431.

[37] Beisner BE, Haydon DT, Cuddington K. Alternative stable states in ecology. Front Ecol Environ 2003;1(7):376–82. http://dx.doi.org/10.1890/1540-9295(2003)001[0376:ASSIE]2.0.CO;2.

[38] Abbott KC, Nolting BC. Alternative (un) stable states in a stochastic predator–prey model. Ecol Complex 2017;32:181–95. http://dx.doi.org/10.1016/j.ecocom.2016.11.004.

[39] Xu L, Zhang F, Zhang K, Wang E, Wang J. The potential and flux landscape theory of ecology. PLoS One 2014;9(1):e86746. http://dx.doi.org/10.1371/journal.pone.0086746.

[40] Cameron M. Finding the quasipotential for nongradient SDEs. Physica D 2012;241(18):1532–50. http://dx.doi.org/10.1016/j.physd.2012.06.005.

[41] Freidlin MI, Wentzell AD. Random perturbations. In: Random perturbations of dynamical systems. Springer; 1998, p. 15–43. http://dx.doi.org/10.1007/978-1-4612-0611-8_2.

[42] Sethian JA, Vladimirsky A. Ordered upwind methods for static Hamilton–Jacobi equations. Proc Natl Acad Sci USA 2001;98(20):11069–74. http://dx.doi.org/10.1073/pnas.201222998.

[43] Sethian JA, Vladimirsky A. Ordered upwind methods for static Hamilton–Jacobi equations: Theory and algorithms. SIAM J Numer Anal 2003;41(1):325–63. http://dx.doi.org/10.1137/S0036142901392742.

[44] Moore CM, Stieha CR, Nolting BC, Cameron MK, Abbott KC. QPot: An r package for stochastic differential equation quasi-potential analysis. 2015, http://dx.doi.org/10.48550/arXiv.1510.07992, arXiv preprint arXiv:1510.07992.

[45] Thomson JA, Burkholder DA, Heithaus MR, Fourqurean JW, Fraser MW, Statton J, et al. Extreme temperatures, foundation species, and abrupt ecosystem change: an example from an iconic seagrass ecosystem. Global Change Biol 2015;21(4):1463–74. http://dx.doi.org/10.1111/gcb.12694.

[46] Dürr D, Bach A. The Onsager-Machlup function as Lagrangian for the most probable path of a diffusion process. Comm Math Phys 1978;60(2):153–70. http://dx.doi.org/10.1007/BF01609446.

[47] Chao Y, Duan J. The Onsager–Machlup function as Lagrangian for the most probable path of a jump-diffusion process. Nonlinearity 2019;32(10):3715. http://dx.doi.org/10.1088/1361-6544/ab248b.

[48] Alkhayuon H, Tyson RC, Wieczorek S. Phase tipping: How cyclic ecosystems respond to contemporary climate. P Roy Soc A 2021;477(2254):20210059. http://dx.doi.org/10.1098/rspa.2021.0059.

[49] Boettiger C, Batt R. Bifurcation or state tipping: Assessing transition type in a model trophic cascade. J Math Biol 2020;80(1):143–55. http://dx.doi.org/10.1007/s00285-019-01358-z.

[50] O'Keeffe PE, Wieczorek S. Tipping phenomena and points of no return in ecosystems: Beyond classical bifurcations. SIAM J Appl Dyn Syst 2020;19(4):2371–402. http://dx.doi.org/10.1137/19M1242884.

[51] Peng X, Lin W. Complex dynamics of noise-perturbed excitatory-inhibitory neural networks with intra-correlative and inter-independent connections. Front. Physiol. 2022;13. http://dx.doi.org/10.3389/fphys.2022.915511.

[52] Schuecker J, Goedeke S, Helias M. Optimal sequence memory in driven random networks. Phys Rev X 2018;8(4):041029. http://dx.doi.org/10.1103/PhysRevX.8.041029.

[53] Holling CS. The functional response of predators to prey density and its role in mimicry and population regulation. Mem Ent Soc Can 1965;97(S45):5–60. http://dx.doi.org/10.4039/entm9745fv.

[54] Hsu S, Huang T. Global stability for a class of predator-prey systems. SIAM J Appl Math 1995;55(3):763–83. http://dx.doi.org/10.1137/S0036139993253201.

[55] Zorzano MP, Mais H, Vázquez L. Numerical solution for Fokker-Planck equations in accelerators. Phys Sec D 1998;113(2):379–81. http://dx.doi.org/10.1016/s0167-2789(97)00292-3.

[56] Zorzano MP, Mais H, Vazquez L. Numerical solution of two dimensional Fokker-Planck equations. Appl Math Comput 1999;98(2–3):109–17. http://dx.doi.org/10.1016/s0096-3003(97)10161-8.

[57] Xie W, Cai L, Xu W. Numerical simulation for a Duffing oscillator driven by colored noise using nonstandard difference scheme. Physica A 2007;373:183–90. http://dx.doi.org/10.1016/j.physa.2006.05.021.

[58] Wang S, Jin X, Huang Z, Cai G. Break-out of dynamic balance of nonlinear ecosystems using first passage failure theory. Nonlinear Dynam 2015;80(3):1403–11. http://dx.doi.org/10.1007/s11071-015-1951-2.

[59] Thomas JW. Numerical partial differential equations: Finite difference methods, Vol. 22. Springer Science & Business Media; 2013, http://dx.doi.org/10.1007/978-1-4899-7278-1.